

Neutrino non-radiative decay and the diffuse supernova neutrino background

Pilar Ivanéz-Ballesteros¹ and M. Cristina Volpe^{2,*}

¹*Université Paris Cité, Astroparticule et Cosmologie, F-75013 Paris, France*

²*CNRS, Université Paris Cité, Astroparticule et Cosmologie, F-75013 Paris, France*

(Dated: September 27, 2022)

We revisit the possibility that neutrinos undergo non-radiative decay. We investigate the potential to extract information on the neutrino lifetime-to-mass ratio from the diffuse supernova neutrino background. To this aim we explicitly consider the current uncertainties on the core-collapse supernova rate and on the fraction of failed supernovae. We present predictions for the Super-Kamiokande+Gd, the JUNO, the Hyper-Kamiokande and the DUNE experiments that should observe the diffuse supernova neutrino background in the near future. We show the importance of identifying the neutrino mass ordering to break possible degeneracies between DSNB predictions in presence of decay and standard physics.

PACS numbers:

I. INTRODUCTION

The vacuum oscillation discovery [1] and the solution of the solar neutrino problem [1–3] represented a breakthrough in neutrino physics. Another milestone was the observation of neutrinos from the explosion of the blue supergiant Sanduleak, giving SN1987A, in the Large Magellanic Cloud [4–6]. This unique observation brought crucial progress on the longstanding open issue of the supernova explosion mechanism as well as on non-standard neutrino properties, particles and interactions.

Past supernovae emitted huge amounts of neutrinos of all flavors which formed a diffuse supernova neutrino background (DSNB) (see [7–9] for reviews). This background, integrated over cosmological time, depends on the still uncertain core-collapse supernova rate and the debated fraction of failed supernovae on the one hand, on flavor mechanisms and unknown neutrino properties on the other.

The Super-Kamiokande (SK) experiment set the first limit on the $\bar{\nu}_e$ flux, i.e. $1.2 \bar{\nu}_e \text{ cm}^{-2}\text{s}^{-1}$ ($E_\nu > 19.3 \text{ MeV}$, 90 % C.L.) [10]. This result was superseded by a subsequent analysis [11] and by the combined analysis of SK-I to SK-IV data which gives the upper limit of $2.8\text{--}3 \bar{\nu}_e \text{ cm}^{-2}\text{s}^{-1}$ ($E_\nu > 17.3 \text{ MeV}$, 90 % C.L.) [12]. The KamLAND experiment and the Borexino Collaboration also obtained limits in the window [8.3, 31.8] MeV [13] and [7.8, 16.8] MeV [14] respectively. As for the relic ν_e flux, the ensemble of SNO results provides the upper limit of $19 \nu_e \text{ cm}^{-2}\text{s}^{-1}$ in the window [22.9, 36.9] MeV (90 % C.L.) [15]. Neutrino-nucleus coherent scattering in dark matter detectors could lower the current limits of $\phi_{\nu_x, \bar{\nu}_x} < 1.3\text{--}1.8 \cdot 10^3 \text{ cm}^{-2}\text{s}^{-1}$ ($E_\nu > 19 \text{ MeV}$) [16] to

$10 \nu_x$ or $\bar{\nu}_x$ (for $x = \mu, \tau$ flavors) [17].

Numerous predictions [18–24] of the DSNB rates are close to the current SK sensitivity limit [12], whereas the most conservative ones lie below by a factor of 2 [25, 26] or 3 to 5 [27, 28]. Beacom and Vagins [29] suggested to add gadolinium (Gd) to SK (SK-Gd) to substantially improve the background suppression. Its inclusion introduces better neutron tagging through the identification of the 8 MeV photons following neutron capture on Gd. The SK-Gd experiment is currently running. With the development of new techniques for background suppression and the advent of the Jiangmen Underground Neutrino Observatory (JUNO) [30], the Hyper-Kamiokande (HK) experiment [31] and the Deep Underground Neutrino Experiment (DUNE) [32] the DSNB discovery should lie in the forthcoming future.

The DSNB detection constitutes a unique *harvest*. Complementary to the neutrino signals from a single supernova, it is sensitive to the star-formation rate and the fraction of failed supernovae [26], evaluated in [27] e.g. on the basis of the metallicity evolution of galaxies. The DSNB receives a contribution from binaries [24, 28, 33, 34] and has a sensitivity to the neutron star equation of state [22] (see [35] for a review).

Moreover, the DSNB depends on neutrino flavor evolution in dense environments. This is a complex open problem that has triggered theoretical investigations since fifteen years (see e.g. [36–39] for reviews). The MSW effect [40, 41] is routinely included in DSNB predictions. In contrast, shock waves, turbulence and $\nu\nu$ neutral-current interactions, which impact the neutrino spectra, have still received little attention in the context of the DSNB. For example, [19] implemented both shock waves and $\nu\nu$ interactions in the so-called *bulb* model and found that their effects could modify the rates by 10 – 20%. Ref. [42] showed that the DSNB rates also depend on the shock wave revival time.

*Electronic address: Corresponding author: volpe@apc.in2p3.fr

The DSNB will be an interesting laboratory for the search of non-standard neutrino properties such as neutrino decay. This property has received attention in studies based on terrestrial experiments, astrophysical sources and on cosmological observables. From atmospheric and long-baseline experiments the lower bound $\tau_3/m_3 > 9.1 \times 10^{-11}$ s/eV (99 % C.L.) was deduced for example by Ref.[43] in the framework of Majoron models. Ref.[44] discussed model independent bounds using solar neutrinos. SNO combined with other solar experiments reported the limit $\tau_2/m_2 > 1.04 \times 10^{-3}$ s/eV (99 % C.L.) [45]. If a supernova explodes at 10 kpc, the observation of the neutronisation burst can tell us if $\tau/m \leq 10^5\text{-}10^7$ s/eV with DUNE and HK [46]. Limits on neutrino invisible two-body decay from SN1987A were also obtained [47, 48]. Several studies used CMB and BBN observations to infer lower bounds. For example Ref.[49] found the constraint $\tau > 0.3 - 1.3$ s $(m/0.05 \text{ eV}^{-1})^3$ (95 % C.L.) with Planck2018 data and $\tau > 10^{-3}$ s (at 95.4 % C.L.) to have a successful BBN.

Usually, investigations of neutrino decay assume that the decaying and the mass eigenstates coincide. Instead, Ref.[50] derived oscillation formulas with neutrino decay including this mismatch. Ref.[51] obtained compact expressions to implement it, using a resummation of the Zassenhaus expansion. The authors pointed out that the inclusion of this correction is relevant in precision experiments of neutrino vacuum oscillations.

The DSNB has a unique sensitivity to neutrino non-radiative two-body decay for $\tau/m \in [10^9, 10^{11}]$ s/eV [52]. Ref.[53] performed a detailed 3ν flavor analysis of non-radiative decay and the DSNB, considering both normal and inverted mass ordering and different mass patterns for the neutrino decay. Using one Fermi-Dirac distribution for the supernova neutrino spectra, the authors evaluated its impact on inverse beta-decay. With the same hypothesis on the supernova neutrino spectra, Ref.[54] considered an effective case of 2ν , in which the heaviest neutrino decays into the lightest, and the intermediate remains stable. For normal ordering and strongly hierarchical mass pattern, the authors gave prospects for HK. Ref.[25] studied neutrino decay using a similar effective 2ν framework, but implementing some progenitor dependence. Combining DSNB rates from different detection channels in JUNO, DUNE and HK, the authors showed the possibility to break some of the degeneracies between the no-decay and the decay cases.

The present manuscript presents a 3ν flavor investigation of the DSNB including neutrino non-radiative two-body decay. Our results go beyond previous works in several respects. First, we explicitly implement the uncertainty coming from the evolving core-collapse supernova rate. Second, we include the progenitor dependence of the supernova neutrino fluxes using inputs from

one-dimensional supernova simulations (from the Garching group) and consider three different scenarios for the black-hole fraction. For flavor evolution, as in previous works, we consider the MSW effect only. Third, we show the influence of neutrino non-radiative decay on the relic neutrino fluxes going from the 2ν to the 3ν framework, for the quasi-degenerate and the strongly-hierarchical mass patterns in the normal or inverted neutrino mass ordering. We present our predictions of the DSNB (integrated) fluxes and number of events for the running SK-Gd experiment and the upcoming HK, JUNO and DUNE experiments. We discuss their potential to extract information on the neutrino lifetime-to-mass ratio.

The manuscript is structured as follows. In Section II we introduce the theoretical framework for the DSNB with neutrino radiative two-body decay. We describe the different ingredients that influence the DSNB flux, in particular the evolving core-collapse supernova rate and the black-hole contribution. Then we introduce the formalism to include neutrino non-radiative decay. Section III presents the numerical results on the DSNB fluxes with/without decay and the expected events in the four experiments. Section IV is the conclusion.

II. THEORETICAL FRAMEWORK

Let us introduce the astrophysical, cosmological and particle physics aspects relevant for the DSNB. We present here our choices for the evolving core-collapse supernova rate, the cosmological model and the supernova neutrino fluxes that include a progenitor dependence. Then we describe the 2ν and 3ν theoretical frameworks used to implement neutrino non-radiative two-body decay.

A. The DSNB flux

The DSNB flux is built up from the neutrino emission of past supernovae that left either a neutron star (NS) or a black hole (BH). In our calculations we assume that neutrinos decay in vacuum, once they have been produced in the supernova core and have undergone spectral swapping, due to the Mikheev-Smirnov-Wolfenstein (MSW) effect, before reaching the star surface.

1. Supernova neutrino fluxes without decay

At the neutrinosphere, the neutrino yields Y_ν are given by quasi-thermal neutrino spectra $\phi_\nu^0(E_\nu)$, normalized to unity ($\int dE_\nu \phi_\nu^0(E_\nu) = 1$). These are characterized by three inputs, i.e. the normalization, the neutrino average

energy and the pinching parameter α . Explicitly, one has

$$Y_\nu = \frac{L_\nu}{\langle E_\nu \rangle} \phi_\nu^0(E_\nu) , \quad (1)$$

with L_ν the total gravitational binding energy emitted by the supernova. The power-law distributions read [55]

$$\phi_\nu^0(E_\nu) = \frac{(\alpha + 1)^{\alpha+1}}{\langle E_\nu \rangle \Gamma(\alpha + 1)} \left(\frac{E_\nu}{\langle E_\nu \rangle} \right)^\alpha e^{-\frac{(1+\alpha)E_\nu}{\langle E_\nu \rangle}} , \quad (2)$$

with α related to the first and second moments of the neutrino energy distribution through the relation

$$\alpha = \frac{\langle E_\nu^2 \rangle - 2\langle E_\nu \rangle^2}{\langle E_\nu \rangle^2 - \langle E_\nu \rangle^2} . \quad (3)$$

When neutrinos traverse the supernova they undergo flavor transformation due to neutrino interactions with the matter and experience the MSW effect [40, 41, 56]. More generally, the presence of shock waves, turbulence and $\nu\nu$ interactions can trigger collective and non-collective flavor mechanisms investigated since many years (see [36, 37, 39, 57] for reviews). The complexity of this problem is such that more work is needed to assess the final impact on the supernova neutrino fluxes. Therefore, we only include here the established MSW effect. As a result, the neutrino yield at the star surface is¹

$$\begin{aligned} Y_{\nu_1} &= Y_{\nu_x} & Y_{\nu_2} &= Y_{\nu_x} & Y_{\nu_3} &= Y_{\nu_e} & \text{(NO)} , \\ Y_{\bar{\nu}_1} &= Y_{\nu_x} & Y_{\bar{\nu}_2} &= Y_{\nu_e} & Y_{\bar{\nu}_3} &= Y_{\nu_x} & \text{(IO)} , \end{aligned} \quad (4)$$

and the antineutrino yield is

$$\begin{aligned} Y_{\bar{\nu}_1} &= Y_{\bar{\nu}_e} & Y_{\bar{\nu}_2} &= Y_{\nu_x} & Y_{\bar{\nu}_3} &= Y_{\nu_x} & \text{(NO)} , \\ Y_{\bar{\nu}_1} &= Y_{\nu_x} & Y_{\bar{\nu}_2} &= Y_{\nu_x} & Y_{\bar{\nu}_3} &= Y_{\bar{\nu}_e} & \text{(IO)} , \end{aligned} \quad (5)$$

with NO standing for normal (i.e. $\Delta m_{13}^2 > 0$) and IO for inverted (i.e. $\Delta m_{13}^2 < 0$) ν mass ordering.

2. Relic supernova neutrino fluxes

The local relic supernova neutrino fluxes for the mass eigenstates ν_i , including a progenitor dependence, read

$$\phi_{\nu_i}(E_\nu) = c \int \int dM dz \left| \frac{dt_c}{dz} \right| R_{\text{SN}}(z, M) Y_{\nu_i}(E'_\nu, M) , \quad (6)$$

with $E_\nu = E'_\nu(1+z)^{-1}$ the redshifted neutrino energy, c the speed of light and $z \in [0, z_{\text{max}}]$ the cosmological redshift. In our calculations, we take $z_{\text{max}} = 5$ and $M \in [8, 125] M_\odot$ as mass range of the supernova progenitors.

The first factor in Eq.(6) is the cosmic time that depends on the cosmological model. In this work, we assume the Λ CDM model² for which the expansion history of the Universe is given by

$$\left| \frac{dz}{dt_c} \right| = H_0(1+z) \sqrt{\Omega_\Lambda + (1+z)^3 \Omega_m} , \quad (7)$$

where H_0 is the Hubble constant, Ω_Λ and Ω_m the dark energy and the matter cosmic energy densities which we take equal to 0.7 and 0.3 respectively. Concerning H_0 , there is currently a tension between the Hubble constant value extracted with the "distance ladder method" and the Cosmological Microwave Background (CMB) [59]. The former gives $H_0 = 74.03 \pm 1.42 \text{ km s}^{-1} \text{ Mpc}^{-1}$, whereas the latter $H_0 = 67.4 \pm 0.5 \text{ km s}^{-1} \text{ Mpc}^{-1}$. For the present work we employ $H_0 = 67.4 \text{ km s}^{-1} \text{ Mpc}^{-1}$, while we have checked that the results are not sensitive to variations of H_0 .

The second important input in Eq.(6) is the evolving core-collapse supernova rate (number per unit time per unit comoving volume) $R_{\text{SN}}(z, M)$ that is related to the star-formation rate history $\dot{\rho}_*(z)$ as

$$R_{\text{SN}}(z, M) = \dot{\rho}_*(z) \frac{\phi(M) dM}{\int_{0.5 M_\odot}^{125 M_\odot} \phi(M) M dM} , \quad (8)$$

where $\phi(M)$ is the initial mass function. The quantity $\phi(M)d(M)$ gives the number of stars in the mass interval³ $[M, M+dM]$. We take the standard power-law introduced by Salpeter [60]

$$\phi(M) \sim M^\chi , \quad (9)$$

with $\chi = -2.35$ for $M \geq 0.5 M_\odot$ (for a discussion on the universality of $\phi(M)$ at higher masses, see for example [61]).

For the star-formation rate history, we employ the piecewise continuous form of a broken power law by [62] (see also [63])

$$\dot{\rho}_*(z) = \dot{\rho}_0 \left[(1+z)^{\alpha\eta} + \left(\frac{1+z}{B} \right)^{\beta\eta} + \left(\frac{1+z}{C} \right)^{\gamma\eta} \right]^{-1/\eta} , \quad (10)$$

with $\alpha = 3.4, \beta = -0.3, \gamma = -3.5$ the logarithmic slopes at low, intermediate and high redshift, $\eta = -10$ the

¹ Since the supernova neutrino fluxes depend on the progenitor, Eqs.(2)-(5) should have an explicit dependence on the progenitor mass M . We have omitted it, in this section, not to overburden the text.

² Note that Ref.[58] investigated the influence of other cosmological models on the DSNB.

³ Note that changing the upper value of the integral from $100 M_\odot$ to $125 M_\odot$ does not introduce significant differences.

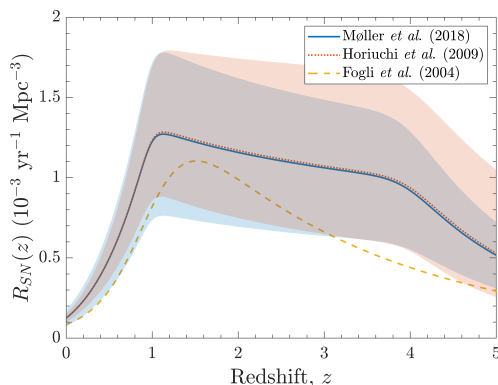


FIG. 1: Core-collapse supernova rate as a function of redshift. The figure shows the piecewise parameterization by [62] and [66], used in [21, 22] (blue), and the one from [65] (pink) with the band showing the core-collapse supernova rate uncertainty. The dashed line shows the older evolving core-collapse supernova rate, employed in the DSNB study of [53], including neutrino (in)visible decay.

smoothing function and $B = 5000$, $C = 9$ the constants defining the redshift breaks (Figure 1). Ref. [64] introduced a modified broken power law for the IMF with $\chi = -1.5$ at $0.1 M_{\odot} \leq M \leq 0.5 M_{\odot}$ and $\chi = -2.12$ for $M > 0.5 M_{\odot}$. It gives a similar $R_{SN}(z, M)$ [65]. Table I presents the values of $\dot{\rho}_0$ and of $R_{SN}(0) = \int_{8 M_{\odot}}^{125 M_{\odot}} R_{SN}(0, M) dM$ (see Eq.(8)). The evolving core-collapse supernova rate impacts the DSNB normalisation and constitutes, at present, the largest source of uncertainties for the DSNB.

The parametrization (10) used in [22], is close but smoother than the one employed by [21]. It differs from the one used in [53] which has been superseded. Ref. [33] obtained a modified parametrization⁴, compared to the one of [62], since the authors considered the subset of the star-formation rate data corrected for extinction by dust. Moreover they argued that the *supernova rate problem*⁵ [66] was only apparent since the core-collapse supernova rate, deduced from the star-formation rate history, could agree with the one from direct core-collapse supernova observations if one included a contribution from binaries, failed supernovae and from (electron-capture) ONeMg supernovae.

The last important factor Eq.(6) are the neutrino fluxes from a single supernova. Taking into account the

	$R_{SN}(0)$	$\dot{\rho}_0$
Low	0.75	0.0054
Fiducial	1.25	0.0089
High	1.75	0.0125

TABLE I: Normalisation of the star-formation rate history (in units of $M_{\odot} \text{ yr}^{-1} \text{ Mpc}^{-3}$) Eq.(10) and local core-collapse supernova rate (in units of $10^{-4} \text{ yr}^{-1} \text{ Mpc}^{-3}$) Eq.(8).

contributions from progenitors with mass M , at redshift z , one has

$$Y_{\nu_i}(E'_{\nu}, M) = f_{NS} Y_{\nu_i, NS}(E'_{\nu}, M) + f_{BH} Y_{\nu_i, BH}(E'_{\nu}, M), \quad (11)$$

with f_{BH} the BH fraction, or $f_{NS} = 1 - f_{BH}$ the NS fraction. Although dark collapses are subdominant, their contribution to the DSNB can be significant, as pointed out by Lunardini [67]. In fact, the compression of baryonic matter, during black hole formation, generates large neutrino fluxes with higher average energies and larger differences among flavors (than optical supernovae) [68], depending on the (soft or stiff) equation of state. Therefore, the black hole contribution impacts the tail of the DSNB flux (see Figure 4). Note that, in the present work, we neglect the dependence of the DSNB flux on the galaxy metallicity, considered for example in [27].

3. Scenarios for the fraction of failed supernovae

Let us now describe three scenarios for the fraction of failed supernovae and introduce what we refer to as *Fiducial*, *Low* and *High*. For the supernova neutrino spectra at the neutrinosphere Eq.(1)-(3), we use fluences of one-dimensional simulations by the Garching group [21, 69], with the Lattimer-Swesty equation of state giving the matter compressibility parameter $K = 220$ (in agreement with nuclear measurements). The progenitors, with solar metallicity, are from Woosley and Weaver. Table I gives their mass and type as well as the neutrino luminosities, average energies and pinching. On the way to the star surface, the spectra are modified by the MSW effect, depending on the neutrino mass ordering Eqs.(4)-(5).

In our scenarios for the black-hole fraction we follow⁶ [21] and [22], and combine the progenitors used in the two works. Obviously a more detailed dependence on the progenitor masses would be desirable. For example, [23, 24, 28] performed extensive supernova simulations to make DSNB predictions. Since our focus here is to investigate non-standard neutrino properties we stick to a

⁴ Note that the parametrization does not hold at $z > 4$ since the authors do not include GRB data, contrary to [62].

⁵ The two disagree by a factor 2 at $0 \leq z \leq 1$.

⁶ Note that BH fractions used in [21, 22] differ from each other.

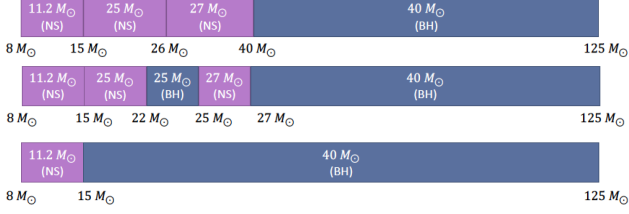


FIG. 2: Scenario I to III (top to bottom) for the BH fraction as well as the progenitor dependence of a supernova that left either a neutron star or a black hole. The parameters (neutrino luminosity, average energies and pinching) of the corresponding fluences are given in Table II.

simpler, but still detailed progenitor dependence, which improves against [46, 53] that used one power law spectrum and to [25] that included either one Fermi-Dirac spectrum, or BH contribution.

Here are the three scenarios (Figure 2):

I- $f_{\text{BH}} = 0.09$ is obtained when all stars that have $M \geq 40 M_{\odot}$ become BH;

II- $f_{\text{BH}} = 0.21$ both stars with $M \in [22, 25] M_{\odot}$ and $M \geq 27 M_{\odot}$ collapse into a BH;

III- $f_{\text{BH}} = 0.41$ is an extreme case where all stars with $M \geq 15 M_{\odot}$ turn into a BH.

Scenario I: This is the most conservative case that we take for comparison with the previous literature (see for example [21, 33]). In this case, we use 4 templates for the supernova progenitors, as [21]. These comprise a $11.2 M_{\odot}$ NS progenitor in the $[8, 15] M_{\odot}$ interval, a $25 M_{\odot}$ and $27 M_{\odot}$ NS cases for the mass ranges $[15, 26] M_{\odot}$ and $[26, 40] M_{\odot}$ respectively, and a $40 M_{\odot}$ BH progenitor for $M_{\odot} \geq 40 M_{\odot}$.

Scenario II: Detailed supernova simulations give the black hole fraction of 0.17, as conservative [24]. Here we take⁷ the $11.2 M_{\odot}$ NS progenitor in the interval $[8, 15] M_{\odot}$, the $25 M_{\odot}$ NS for $[15, 22] M_{\odot}$, the $25 M_{\odot}$ BH case in $[22, 25] M_{\odot}$, the $27 M_{\odot}$ NS in the $(25, 27) M_{\odot}$ interval and the $40 M_{\odot}$ BH progenitor above $27 M_{\odot}$.

Scenario III: This is most optimistic case, in agreement with simulations [24]. We implement the $11.2 M_{\odot}$ NS for the $[8, 15] M_{\odot}$ interval and the $40 M_{\odot}$ BH progenitor for $M_{\odot} \geq 15 M_{\odot}$.

The case with $f_{\text{BH}} = 0.21$ and $R_{\text{SN}}(0) = 1.25 \pm 0.5 \cdot 10^{-4} \text{ yr}^{-1} \text{ Mpc}^{-3}$ is our *Fiducial* DSNB model. The *Low*

Run Type	$\langle E_{\nu_e} \rangle$	$\langle E_{\bar{\nu}_e} \rangle$	$\langle E_{\nu_x} \rangle$	α_{ν_e}	$\alpha_{\bar{\nu}_e}$	α_{ν_x}	L_{ν_e}	$L_{\bar{\nu}_e}$	L_{ν_x}
s11.2c NS	10.43	12.89	12.93	2.99	2.79	2.30	3.56	3.09	3.02
25.0c NS	12.67	15.5	15.41	2.61	2.79	2.30	7.18	6.78	6.02
25.0c BH	15.32	18.2	17.62	3.21	3.21	2.16	7.08	6.51	3.7
27 NS	11.3	13.89	13.85	2.79	2.45	2.16	5.87	5.43	5.1
40.0c BH	15.72	18.72	17.63	2.79	2.79	1.92	9.38	8.6	4.8

TABLE II: The first two columns give the run and type of the $11.2 M_{\odot}$, $25 M_{\odot}$, $27 M_{\odot}$ and $40 M_{\odot}$ progenitors used in the DSNB predictions. The other columns provide the corresponding average energies (MeV), pinching parameters and luminosities (10^{52} erg) defining the supernova neutrino fluences Eq.(2) of the different neutrino flavors. The values are obtained from one-dimensional supernova simulations of the Garching group [21, 69].

and *High* scenarios correspond to the variability of the local core-collapse supernova rate (see Section II.A.2 and Table I).

B. Neutrino (in)visible two-body decay

Having presented the main ingredients of the DSNB flux, we now describe how to extend the standard framework to include neutrino (in)visible two-body decay. We consider the processes where a heavy neutrino ν_i decays into a lighter one ν_j and a massless, or almost massless, scalar particle ϕ , i.e.

$$\nu_i \rightarrow \nu_j + \phi \quad \text{or} \quad \nu_i \rightarrow \bar{\nu}_j + \phi. \quad (12)$$

Neutrino decay to Majorons has been discussed in the context of various models (see for example [70]). The new degrees of freedom are singlets under the Standard Model gauge group. In the case of Dirac neutrinos, the decay requires dimension five (lepton-number zero) or four and six (lepton-number two) operators. For Majorana neutrinos the minimal interaction that leads to the neutrino decay has dimension six [46]

$$\mathcal{L}_{\text{Maj}} \supset \frac{\tilde{g}_{ij}}{2\Lambda^2} (L_i H) (L_j H) \phi + \text{h.c.} \supset g_{ij} (\nu_L)_i (\nu_L)_j \phi + \text{h.c.}, \quad (13)$$

where $\tilde{g}_{ij} = \tilde{g}_{ji}$ and $g_{ij} = \tilde{g}_{ij} v^2 / \Lambda^2$, L, H are the Standard Model lepton doublets and Higgs field, v is the vacuum expectation value of the neutral component of the Higgs field, ν is the neutrino field. Since here we do not wish to focus on specific models, we will keep our considerations general.

The (rest-frame) neutrino lifetime and associated decay rate receive contributions from both processes (12),

⁷ Note that the shortage of optical supernovae in the $[17, 25] M_{\odot}$ window could be related to the *red supergiant problem* (see [65]).

that is

$$\tau_{\nu_i}^{-1} = \tilde{\Gamma}_{\nu_i} = \sum_{m_j < m_i} \tilde{\Gamma}(\nu_i \rightarrow \nu_j) + \tilde{\Gamma}(\nu_i \rightarrow \bar{\nu}_j) . \quad (14)$$

The related decay rate in the laboratory frame reads

$$\Gamma_{\nu_i} = \frac{m_i}{E_\nu} \tilde{\Gamma}_{\nu_i} , \quad (15)$$

with m the absolute neutrino mass. Since the value of m is not known yet, studies on ν non-radiative decay give limits for τ/m , the lifetime-over-mass ratio. In the following, we shall present our results as a function of τ/m , which also facilitates the comparison with previous works. Finally the branching ratios are

$$B_{\nu_i} = \Gamma(\nu_i \rightarrow \nu_j) / \Gamma_{\nu_i} , \quad (16)$$

and similarly for $\nu_i \rightarrow \bar{\nu}_j + \phi$.

1. Neutrino kinetic equations in presence of (in)visible decay

The generic form of the kinetic equations for ultra-relativistic neutrinos including neutrino decay is [53]

$$\mathcal{L}[n_{\nu_i}(E_\nu, t)] = \mathcal{C}[n_{\nu_i}(E_\nu, t)] , \quad (17)$$

where $n_{\nu_i}(E_\nu, t)$ is the relic number density of the ν_i mass eigenstates ($i = 1, 2, 3$) (per unit energy and comoving volume) at time t , related to the phase space distribution function f through $n_{\nu_i}(E_\nu, t) = 4\pi p^2 f(R(t)/R_0)^3$ ($R(t)$ is the universe scale factor of the Friedman-Robertson-Walker metric and $E_\nu \approx p = |\vec{p}|$). The Liouville operator then reads

$$\mathcal{L}[n_{\nu_i}(E_\nu, t)] = [\partial_t - H(t)E_\nu \partial_E - H(t)] n_{\nu_i}(E_\nu, t) , \quad (18)$$

with $H(t)$ the Hubble constant. The explicit expression of the collision term in Eq.(17) for decaying neutrinos⁸ is

$$\begin{aligned} \mathcal{C}[n_{\nu_i}(E_\nu, t)] = & R_{\text{SN}}(t) Y_{\nu_i}(E_\nu) + \sum_{m_i > m_j} q_{ij}(E_\nu, t) \\ & - \Gamma_{\nu_i} n_{\nu_i}(E_\nu, t) , \end{aligned} \quad (19)$$

with

$$q_{ij}(E_\nu, t) = \int_{E_\nu}^{\infty} dE'_\nu n_{\nu_i}(E'_\nu, t) \Gamma_{\nu_i} \psi_{ij}(E'_\nu, E_\nu) . \quad (20)$$

where $\psi_{ij}(E'_\nu, E_\nu)$ are the neutrino decay energy spectra. The first contribution in the collision term Eq.(19) is the usual one from core-collapse supernovae (without decay). The second source term accounts for the feeding of the lighter states ν_j from the decay of the heavier ones ν_i . The last is a sink term which implements the ν_i decay loss with total decay rate Γ_{ν_i} Eq.(14) which is present for the heavier neutrinos only.

After performing a change of variables from (t, E_ν) to the redshift and (redshifted) neutrino energies (z, E'_ν) , one can rewrite Eqs.(17)-(20) and obtain the general solution for the relic number of neutrinos (per unit of comoving volume and of energy at redshift z) [53] that is

$$\begin{aligned} n_{\nu_i}(E_\nu, z) = & \frac{1}{1+z} \int_z^\infty \frac{dz'}{H(z')} \left[R_{\text{SN}}(z') Y_{\nu_i} \left(E_\nu \frac{1+z'}{1+z} \right) \right. \\ & \left. + \sum_{m_i > m_j} q_{ij} \left(E_\nu \frac{1+z'}{1+z}, z' \right) \right] e^{-\Gamma_{\nu_i} [\chi(z') - \chi(z)](1+z)} , \end{aligned} \quad (21)$$

where the auxiliary function $\chi(z)$ is

$$\chi(z) = \int_0^z dz' H^{-1}(z') (1+z')^{-2} . \quad (22)$$

This result reduces to the standard expression Eq.(6) when $\Gamma = 0$ (in the limit $\tau \rightarrow \infty$). To determine the DSNB fluxes and the associated rates in the full 3ν framework, one exploits the general solution Eq.(21) for $z = 0$, with Eqs.(20) and (22).

2. 2ν and 3ν decay patterns

In order to investigate the role of processes (12), it is necessary to define the neutrino mass patterns and the branching ratios B_{ν_i} Eq.(16) of the heavier mass eigenstates m_h decaying to the lightest m_l . Following the 3ν study [53], we consider two (extreme) possibilities:

- i) QD: a quasi-degenerate mass pattern, where $m_h \simeq m_l \gg m_h - m_l$;
- ii) SH: a strongly hierarchical mass pattern, where $m_h \simeq m_l \gg m_l \simeq 0$.

Note that Refs.[25, 46] considered 2ν decay in the SH scenario only. In the 2ν flavor framework, one has either the QD case with $B(\nu_2 \rightarrow \nu_1) = 1$ and $B(\nu_2 \rightarrow \bar{\nu}_1) = 0$ or the SH case with $B(\nu_2 \rightarrow \nu_1) = B(\nu_2 \rightarrow \bar{\nu}_1) = 1/2$ (see for example [70]).

Figure 2 presents the decay schemes and the associated branching ratios for 3ν flavors. The figure shows the cases for NO mass patterns, either with SH (top figure) or with QD (middle figure). The IO mass pattern (lower

⁸ In this section, the explicit dependence on the progenitor mass M is not included not to overburden the text.

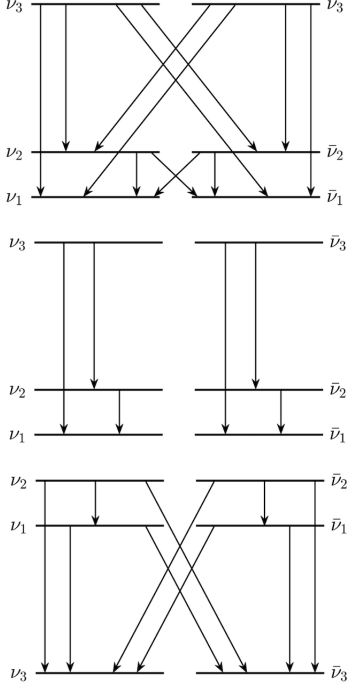


FIG. 3: Decay patterns for 3ν flavors. Top: Normal mass ordering in the strongly-hierarchical (SH) case. The branching ratios are equal to $1/4$ for ν_3 ($\bar{\nu}_3$) and $1/2$ for ν_2 ($\bar{\nu}_2$). Middle: Normal mass ordering in the quasi-degenerate case (QD). The branching ratios are equal to $1/2$ for ν_3 or $\bar{\nu}_3$. Bottom: Inverted mass ordering case. The branching ratios are equal to $1/3$ for ν_2 ($\bar{\nu}_2$) and $1/2$ for ν_1 ($\bar{\nu}_1$). In all cases the lifetime-to-mass ratio of the decaying eigenstates is taken equal, i.e. $\tau_2/m_2 = \tau_3/m_3$ (NO) or $\tau_2/m_2 = \tau_1/m_1$ (IO).

figure) comprises a SH and a QD patterns as subsystems. For the computations we use a *democratic* hypothesis for $B(\nu_i \rightarrow \nu_j)$ (see the caption of Figure 2) and assume equal lifetime-to-mass ratio for the decaying eigenstates. This choice does not employ specific *ansatz* and has the advantage of reducing the number of free parameters.

The last piece that needs to be specified are the neutrino decay energy spectra Eq.(20). In the QD case, one has [46, 53]

$$\psi(E_{\nu_h}, E_{\nu_l}) = \delta(E_{\nu_h} - E_{\nu_l}). \quad (23)$$

On the contrary, in the SH case, both helicity changing (h.c.) and flipping (h.f.) decays contribute to the neutrino decay rate with neutrino spectra

$$\psi_{\text{h.c.}}(E_{\nu_h}, E_{\nu_h}) = \frac{2E_{\nu_l}}{E_{\nu_h}^2} \quad \psi_{\text{h.f.}}(E_{\nu_h}, E_{\nu_l}) = \frac{2}{E_{\nu_h}} \left(1 - \frac{E_{\nu_l}}{E_{\nu_h}}\right). \quad (24)$$

Therefore h.c. contribution produce neutrinos with harder spectra than the h.f. one.

Finally, the total decay rate⁹, in the laboratory frame, for the process (12), e.g. for a ν_3 decaying to ν_1 , is

$$\Gamma(E_{\nu_3}) = \frac{g^2}{32\pi} \frac{m_3^2}{E_{\nu_3}} = \frac{1}{\tau_3} \frac{m_3}{E_{\nu_3}}. \quad (25)$$

III. NUMERICAL RESULTS

We present now our results in the 2ν and 3ν frameworks for the DSNB fluxes and number of events, in absence and in presence of ν non-radiative two-body decay. We make predictions for the running SK-Gd and upcoming water Cherenkov detector HK, the JUNO scintillator and the DUNE liquid argon detectors. We consider three values of the lifetime-over-mass ratio, namely

- $(\tau/m)_{\text{short}} = 10^9 \text{ s/eV};$
- $(\tau/m)_{\text{medium}} = 10^{10} \text{ s/eV};$
- $(\tau/m)_{\text{long}} = 10^{11} \text{ s/eV};$

The $(\tau/m)_{\text{short}}$ case corresponds to almost complete neutrino decay, whereas $(\tau/m)_{\text{long}}$ is close to the upper bound that one gets with (the rule of thumb) [53]

$$\tau/m \leq H_0^{-1} \sim O(10^{11}) \text{ s/eV} \quad (26)$$

for typical supernova neutrino energies.

A. The DSNB fluxes with and without decay

Let us first look at the results on the relic supernova neutrino fluxes of flavor α that are connected to the ones in the mass eigenstate basis according to

$$\phi_{\nu_\alpha}(E_\nu) = \sum_i |U_{\alpha i}|^2 \phi_{\nu_i}(E_\nu), \quad (27)$$

where U is the Pontecorvo-Maki-Nakagawa-Sakata unitary matrix that relates the neutrino flavor and mass basis, i.e. $|\nu_\alpha\rangle = \sum_i U_{\alpha i}^* |\nu_i\rangle$ ($\alpha = e, \mu, \tau$). For 3ν flavors the matrix depends on three neutrino mixing angles, one Dirac and two Majorana CP violating phases. The latter are still unknown. For our calculations we employ $\theta_{23} \approx 45^\circ$, $\theta_{12} \approx 34^\circ$ and $\theta_{13} \approx 8.5^\circ$ as values of the neutrino mixing angles¹⁰ [71]. Note that, there are hints

⁹ Note that there is a factor of 2 missing in Eq. (2.6) of [46]. Note also that g_{ij} should be $g_{ij}/2$ in Eq.(2.1) of [72].

¹⁰ Note that in the 3ν flavor study of [53] $\theta_{13} = 0^\circ$ and therefore $U_{e3} = 0$.

at 2.5σ in favor of the normal mass ordering and for a Dirac phase such that $\sin \delta < 0$ (both at 90 % C.L.) [73].

Let us first consider the DSNB fluxes for ν_e , $\bar{\nu}_e$ and of all flavors added, in absence of neutrino decay for NO and for IO (Figure 4). These results are obtained with the core-collapse supernova rate Eq.(8)-(10) and the three scenarios for the BH fractions $f_{\text{BH}} = 0.09, 0.21, 0.41$ described above. The parameters defining the neutrino fluences (at the neutrinosphere) are shown in Table II. The band in Figure 4 corresponds to the uncertainty in the evolving core-collapse supernova rate (Table I). As one can see from the Figure, our results for the DSNB fluxes agree well with those of [22] (*cfr.* Figure 3). We remind that here we included the $25 M_\odot$ NS and BH cases as well, as in [21].

Before giving our results when neutrinos decay in the 3ν framework, let us look at the differences that arise when only 2ν flavors are considered¹¹. Figure 5 compares the DSNB $\bar{\nu}_e$ fluxes without decay with those corresponding to the shortest and medium lifetime-over-mass ratios, for NO (top) or IO (bottom).

As one can see from the figure, for NO and SH scenario, predictions for the DSNB $\bar{\nu}_e$ fluxes are indistinguishable with the effective 2ν (that is, leaving the second mass eigenstate as stable) or a 3ν framework. This result supports the findings of, for example, [25, 46] where 2ν flavors are considered with NO and SH pattern only. We also find that, for NO and a QD mass pattern, the DSNB flux predictions are practically the same with 2ν or 3ν . As for IO, the predictions based on 2ν or 3ν flavors are very close with $(\tau/m)_{\text{medium}}$ (above 15 MeV) and $(\tau/m)_{\text{long}}$ (not shown). On the contrary, if one considers 2ν and 3ν flavors, this introduces significant differences between the DSNB flux predictions for $(\tau/m)_{\text{medium}}$, below 20 MeV, and for $(\tau/m)_{\text{short}}$, as one can see from Figure 5.

Figures 6, 7 and 8 present the DSNB fluxes in presence of neutrino decay obtained by solving Eq.(21). In the 3ν framework, the DSNB flux behaviors we find are in concordance with those of [53] although they employed an earlier core-collapse supernova rate (see Figure 1), one effective Fermi-Dirac distribution for the supernovae neutrino spectra and no progenitor dependence (as common for predictions at that time).

Figure 6 shows the DSNB $\bar{\nu}_e$ fluxes for NO in the SH case. The ν_e ones are close and follow a similar behavior. As in [53], we find an enhancement of the DSNB fluxes for $(\tau/m)_{\text{short}}$. In fact, at low energy, the ν_e and $\bar{\nu}_e$ fluxes receive a significant contribution from ν_2 and ν_3

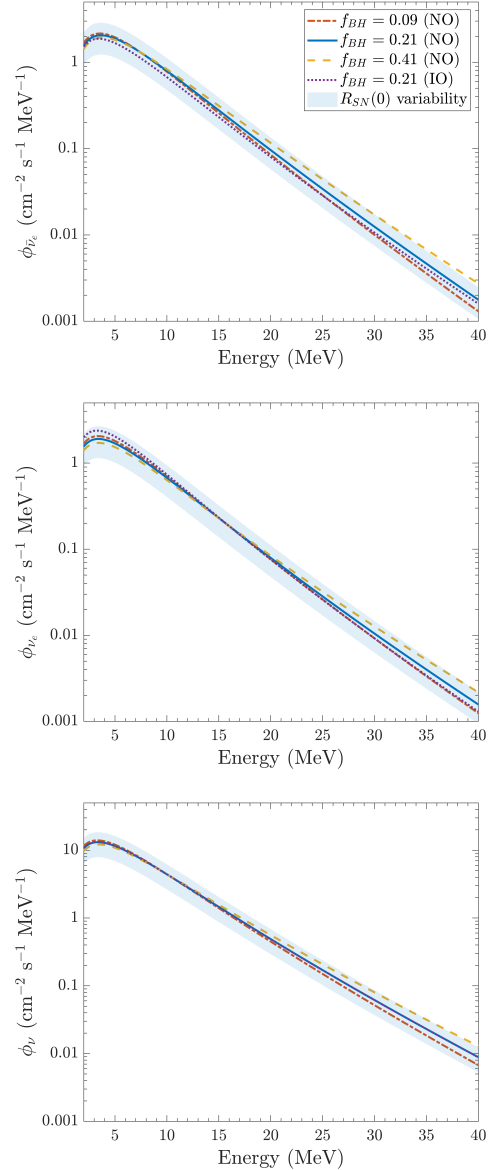


FIG. 4: No ν decay: DSNB fluxes for electron neutrinos (top), electron anti-neutrinos (middle) and all neutrino flavors added (bottom) as a function of neutrino energy, with the Λ CDM model and the core-collapse supernova rate Eq.(8). Three different scenarios are taken for the BH fraction. The NO results correspond to the *Fiducial* model ($f_{\text{BH}} = 0.21$), the band showing the uncertainty from R_{SN} (see Table I). The IO results are for the *Fiducial* model without the R_{SN} uncertainty.

decays that dominate over the contribution of the first term of Eq.(21). Even if this enhancement, present for $(\tau/m)_{\text{short}}$ and for $(\tau/m)_{\text{medium}}$ in particular, is interesting, it appears well below the current energy thresholds. Unfortunately, it will be hard to see such an increase,

¹¹ We show the results for $\bar{\nu}_e$. The difference between ν_e and $\bar{\nu}_e$ relic fluxes is discussed in 3ν framework.

even considering lower energy thresholds due to improvements in background suppression (from e.g. the reduction of atmospheric spallation products like ^9Li in SK-Gd and HK). For $(\tau/m)_{\text{short}}$ the flux is slightly suppressed at higher energies.

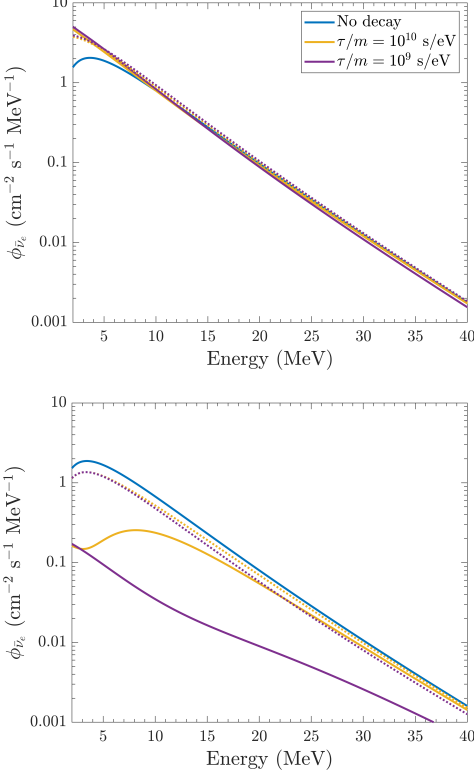


FIG. 5: Comparison of the DSNB $\bar{\nu}_e$ fluxes in presence of ν decay, with 2ν (dotted) or 3ν (full lines), for NO, SH (top) and IO (bottom). Only $(\tau/m)_{\text{short}}$ and $(\tau/m)_{\text{medium}}$ are presented for clarity. The DSNB fluxes in absence of decay are also shown. The results correspond to the *Fiducial* model.

The NO and the QD case show different flux behaviors, compared to the SH one (Figure 7) since the first term dominates over the second in Eq.(21). The DSNB ν_e flux differs from the $\bar{\nu}_e$ one, only below 10 MeV. This difference comes from the different spectra at the neutrinosphere. One can also see that, when the uncertainty in the evolving core-collapse supernova rate is included, the results for the *Fiducial* model with no decay significantly overlap, in the DSNB detection window, with those for $(\tau/m)_{\text{short}}$. Clearly, with the present knowledge, flux modifications due to neutrino (in)visible decay would be hidden by such an uncertainty in NO with SH and QD mass patterns.

The situation is different in IO (Figure 3, bottom). The corresponding DSNB fluxes with neutrino decay present interesting features, as can be seen from Figure 8. We

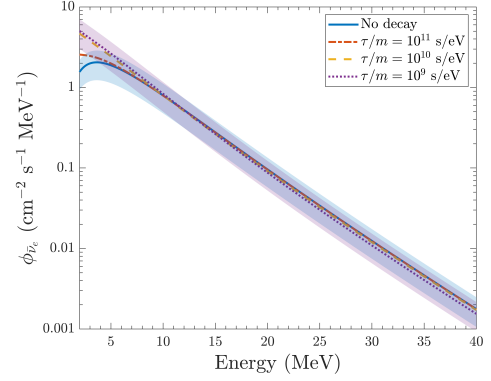


FIG. 6: Neutrino decay in 3ν framework: DSNB $\bar{\nu}_e$ fluxes for NO with the SH decay pattern (Figure 3, top). Three values of the lifetime-over-mass ratio are considered. The lines show the results for the *Fiducial* model, whereas the bands come from the uncertainty on core-collapse supernova rate Eq.(8) (see Table I). The DSNB fluxes in absence of neutrino decay are given for comparison.

give the results for $\bar{\nu}_e$, since the DSNB ν_e fluxes (*Fiducial* model) are the same (for the above-mentioned reason). First of all one can see a significant suppression of the fluxes for $(\tau/m)_{\text{short}}$, whereas the ones for $(\tau/m)_{\text{long}}$ are equivalent (above 10 MeV) to the no decay case. The results with $(\tau/m)_{\text{medium}}$ are close to the no decay results above 15 MeV, whereas below they show a suppression up to a factor of 6, compared to the fiducial no decay case.

Interestingly, for IO, the $(\tau/m)_{\text{short}}$ and no decay cases differ significantly in the full DSNB detection window, even considering the current core-collapse supernova normalization uncertainty. This suppression is due to the fact that, for IO, the DSNB $\bar{\nu}_e$ flux receives a small contribution ($|U_{e3}|^2 = 2 \times 10^{-2}$) from the stable $\bar{\nu}_3$ and large from ν_1 ($\bar{\nu}_1$) and ν_2 ($\bar{\nu}_2$). We shall discuss its implication on the DSNB events in the following section.

Let us now discuss the DSNB integrated $\bar{\nu}_e$ and ν_e fluxes for NO (IO) without decay, in comparison with current bounds (Table III). We consider both the *Fiducial* model and an optimistic prediction with $f_{\text{BH}} = 0.41$. The theoretical errors correspond to the core-collapse supernova rate uncertainty. Our values are below the $\bar{\nu}_e$ upper limit, obtained from the combined analysis of SK-I to SK-IV data [12], by a factor 2 to 4. Note that the KamLAND experiment obtained the upper value of $139 \text{ cm}^{-2}\text{s}^{-1}$ (90 % C.L.) in the window [8.3, 31.8] MeV [13]; slightly improved in the interval [7.8, 16.8] MeV by the model-dependent limit of $112.3 \text{ cm}^{-2}\text{s}^{-1}$ (90 % C.L.) of the Borexino Collaboration [14]. For the integrated DSNB ν_e flux, as can be seen from Table III, the predictions are lower, by about two orders of magnitude,

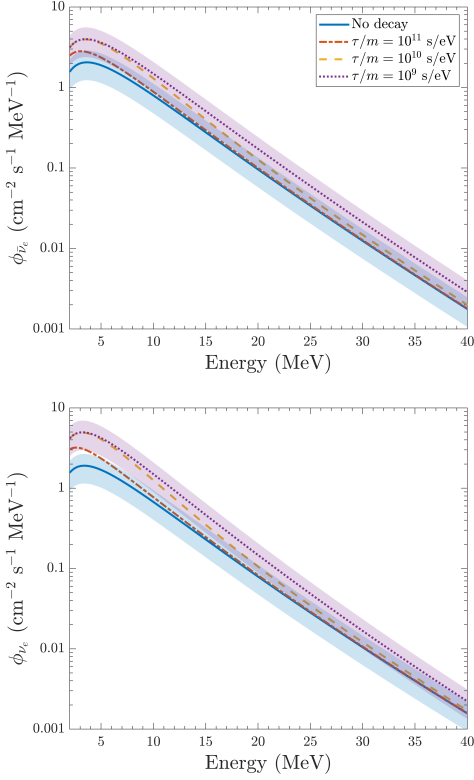


FIG. 7: Same as Figure 6 but for the DSNB $\bar{\nu}_e$ and ν_e fluxes in NO, with the QD decay pattern (Figure 3, middle).

	NO	IO	Upper limits
$\bar{\nu}_e$	0.77 ± 0.30	0.63 ± 0.25	2.8-3 (SK)
	1.02 ± 0.41	0.75 ± 0.3	
ν_e	0.20 ± 0.08	0.18 ± 0.08	19 (SNO)
	0.24 ± 0.9	0.23 ± 0.9	

TABLE III: Integrated DSNB fluxes ($\text{cm}^{-2}\text{s}^{-1}$) for the *Fiducial* model and the optimistic case with $f_{\text{BH}} = 0.41$, in comparison with the current upper limits. Our results are for the case of no-decay and for the two mass orderings. The theoretical errors come from the core-collapse supernova rate uncertainty. The experimental upper limits (90 % C.L.) are from SK-I to SK-IV [12] and SNO [15] with the DSNB windows of $E_\nu > 17.3$ MeV (positron energy) and [22.9, 36.9] MeV (neutrino energy) respectively.

than the current bound deduced from the ensemble of SNO data [15].

Table IV shows the integrated supernova relic fluxes for $\bar{\nu}_e$ and ν_e without/with decay for the SK-Gd, HK, JUNO and DUNE experiments and the related DSNB detection windows. Different values of τ/m are considered as well as the three decay patterns of Figure 3. As

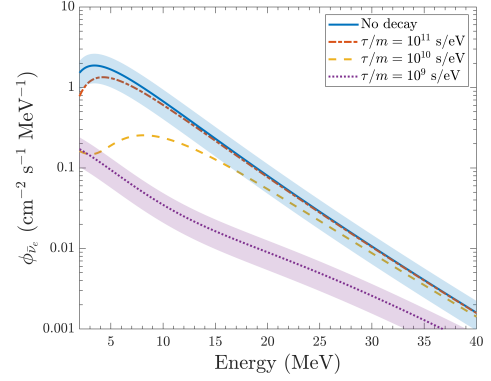


FIG. 8: Same as Figure 6 for the DSNB $\bar{\nu}_e$ fluxes in IO. The corresponding decay mass pattern is shown in Figure 3 (bottom).

expected (Figures 6-8), the integrated DSNB fluxes have little sensitivity to τ/m for NO and the SH pattern. On the contrary, they increase by a factor of 1.8 from no decay to the $(\tau/m)_{\text{short}}$ case for NO and QD. For IO, a significant decrease is obtained, as expected, going from a factor of about 6.7 in DUNE to about 14 in SK-Gd, HK and JUNO for $(\tau/m)_{\text{short}}$. For $(\tau/m)_{\text{medium}}$, the suppression grows from 40 % (DUNE) to a factor of 2 (HK).

B. Predictions of the DSNB events

The DSNB total rates in a detector on Earth are

$$N_\alpha = \epsilon N_t \int dE_\nu \phi_{\nu_\alpha}(E_\nu) \sigma(E_\nu), \quad (28)$$

where ϵ is the detector efficiency (in a given detection channel), N_t is the number of targets (active volume) and $\sigma(E_\nu)$ is the reaction cross section of the associated neutrino detection channel.

Let us remind that SK is a 50 kton water (22.5 kton fiducial volume) Cherenkov detector located in the Kamioka mine in Japan. SK-Gd is running since 2021 and has three phases, with a Gd concentration that increases from 0.01 % (phase I), 0.03 % (phase II) to the ultimate 0.2 % (phase III) reaching 90 % efficiency in neutron tagging. It will be running until the start of HK (approximately ten years).

Located at Tochibora site, HK will be the largest water Cherenkov detector with 258 ktons and a fiducial volume 8.4 times the one of SK. Construction has started early 2020 and the detector is expected to start operating in 2027. Numerous aspects relevant for the DSNB are currently under study, such as the PMT coverage of

	DSNB Flux ($\text{cm}^{-2} \text{s}^{-1}$)			
	No decay	$(\tau/m)_{\text{long}}$	$(\tau/m)_{\text{medium}}$	$(\tau/m)_{\text{short}}$
SK-Gd ($\bar{\nu}_e$) (12.8, 30.8)	2.05 (1.71)	2.16 [2.03] (1.62)	2.87 [1.96] (1.02)	3.72 [1.92] (0.12)
HK ($\bar{\nu}_e$) (8.8, 30.8)	4.81 (4.05)	5.22 [4.79] (3.74)	7.32 [4.71] (1.90)	8.86 [4.79] (0.28)
HK-Gd ($\bar{\nu}_e$) (11.3, 31.3)	2.83 (2.37)	3.02 [2.81] (2.23)	4.08 [2.72] (1.32)	5.17 [2.71] (0.20)
JUNO ($\bar{\nu}_e$) (11.3, 33.3)	2.85 (2.38)	3.03 [2.83] (2.24)	4.1 [2.74] (1.33)	5.2 [2.72] (0.20)
DUNE (ν_e) (19, 31)	0.43 (0.40)	0.45 [0.43] (0.39)	0.55 [0.41] (0.29)	0.77 [0.38] (0.06)

TABLE IV: Integrated DSNB fluxes for the *Fiducial* model with $f_{\text{BH}} = 0.21$, in absence and in presence of neutrino non-radiative decay. The results are obtained in the 3ν framework. The first column gives the experiment and the expected DSNB detection window (in MeV) used in our calculations. For the results with neutrino decay, three values of the neutrino lifetime-over-mass ratio are shown: $\tau/m = 10^9$ s/eV (*short*), 10^{10} s/eV (*medium*) and 10^{11} s/eV (*long*). For each experiment, the upper values correspond to NO, QD; the middle ones to NO, SH (in brackets) and the lower ones to IO (in parenthesis). For comparison, results for stable neutrinos are also shown.

the detector, or algorithms to reduce contributions from spallation due to atmospheric backgrounds. The possibility to add Gadolinium is also under study [74].

JUNO, with 20 ktons, will be the largest underground scintillator detector. It will be located at Jiangmen in South China and will be online in 2023 [75]. Techniques are being developed for the DSNB detection, in particular concerning background reduction with the pulse shape analysis [30].

Finally the DUNE experiment will comprise 40 ktons liquid argon (fiducial volume) with 4 far TPC modules at the Sanford Underground Research Facility in South Dakota [32]. The backgrounds and the efficiency of the detector relevant for low energy DSNB events are under investigation.

In order to study the role of neutrino decay on the DSNB rates, we consider the main detection channels for the Cherenkov and scintillator detectors, that is inverse beta-decay (IBD)

$$\bar{\nu}_e + p \rightarrow n + e^+, \quad (29)$$

with $E_{e^+} = E_{\bar{\nu}_e} - \Delta_{np}$, $\Delta_{np} = 1.293$ MeV and a low energy threshold $E_{\bar{\nu}_e} > 1.806$ MeV. For the DUNE experiment the main detection channel is the charged-current

	N_t (10^{33})	ϵ	Time (years)	DSNB window (MeV)	DSNB events
SK-Gd	1.5	57.5%	2	(12.8,30.8)	2 (2) $\bar{\nu}_e$
"	"	73.75%	8	"	12 (10) $\bar{\nu}_e$
HK	12.5	25%	20	(8.8,30.8)	128 (107) $\bar{\nu}_e$
HK-Gd	12.5	40 %	20	(11.3, 31.3)	163 (136) $\bar{\nu}_e$
JUNO	1.21	50%	20	(11.3, 33.3)	20 (17) $\bar{\nu}_e$
DUNE	0.602	86%	20	(19, 31)	12 (11) ν_e

TABLE V: Number of targets (fiducial volume), efficiency, running time and energy window in which the DSNB detection is expected for the running SK-Gd and upcoming HK Cherenkov detectors [12], the scintillator detector JUNO [75] and the liquid argon TPC (LArTPC) far detectors in DUNE [32]. For SK-Gd the two efficiencies correspond to 0.01 % and 0.03 % Gd concentration (phases I and II). For HK we also consider a Gd-doped case, currently under study [74]. The DSNB expected events are also shown, for the case of no decay, in NO (IO).

neutrino-argon interaction

$$\nu_e + {}^{40}\text{Ar} \rightarrow e^- + {}^{40}\text{K}^*. \quad (30)$$

We employ the IBD cross section from [76] for the former and the ν_e -Ar cross section from [77] for the latter.

Table IV gives the parameters (number of targets in the fiducial volume, efficiency, expected DSNB detection window) as well as the running time of the four experiments, which we use to predict the rates. The Table also presents the expected DSNB number of events if neutrinos are stable. Note that for SK-Gd we consider two running periods due to the improved efficiency from increased Gd concentration. We keep the same DSNB detection window for the two periods even though the threshold energy might be lowered thanks to Gd addition. For HK we consider conservative detection efficiencies and windows without and with Gd [74]. For JUNO and DUNE we follow [75] and [25] for the efficiencies and the detection windows.

Let us first look at the differences in the predictions of the DSNB rates from a 2ν instead of a 3ν framework. Figure 8 shows a comparison of the expected number of events with 2ν (dotted) and 3ν (full lines), as a function of positron energy, for the three lifetime-over-mass ratios and for the case of no decay. The results shown are for HK as an example. (Similar trends are found for the other experiments.) For NO, one can see that, while the events are underestimated in the QD case, they are overestimated in the SH one. The latter is on par with the different trends in the fluxes already observed in Figure 5.

On the contrary, the event predictions with 2ν and 3ν are strikingly different for IO, in particular for the shortest τ/m . For $(\tau/m)_{medium}$, in the 2ν case, the events below 16 MeV (positron energy) overestimate the ones with 3ν decay by more than a factor of 2.

More quantitatively, if one uses the effective 2ν , instead of 3ν decay, for $(\tau/m)_{long}$ the total number of events differs by a few up to about 10% (for both mass orderings) in the four experiments. For $(\tau/m)_{medium}$, variations range from a few percent (SK-Gd, HK, JUNO) to 13 % for NO (SH or QD), or almost 30 % (SK-Gd, DUNE) and 50 % (HK) for IO. Moreover, as expected from the DSNB flux results shown in Figure 5, the largest differences appear for $(\tau/m)_{short}$. In particular, these vary from 15-20 % in NO (SH or QD) to a factor of 4.5 (DUNE), 6 (JUNO), 7 (SK-Gd) and 8 (HK). Clearly, if nature has opted for the inverted mass ordering, one should employ a 3ν treatment to learn about neutrino decay.

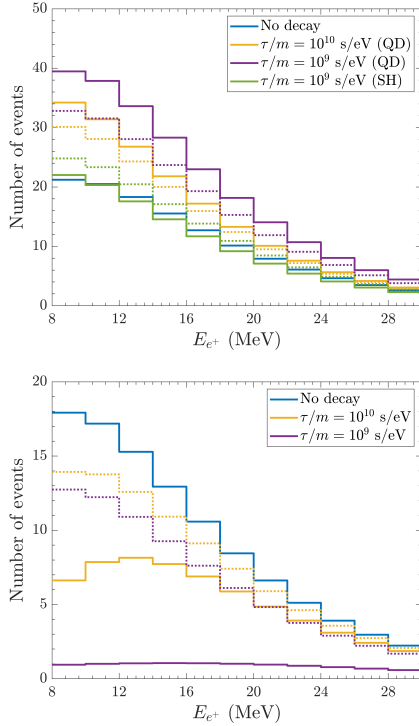


FIG. 9: Comparison of the expected DSNB events, as a function of positron energy, in the 2ν (dotted) and the 3ν frameworks (full lines). The results are for the HK detector and a running time of 20 years for NO (upper) and IO (lower figure). The events for no decay are also shown for comparison.

Let us now discuss the DSNB differential number of $\bar{\nu}_e$ IBD events, as a function of energy, expected in SK-Gd (Figure 10 and 11), HK (Figure 12 and 13) and in JUNO (Figure 14) as well as the $\nu_e + {}^{40}\text{Ar}$ events expected in

Experiment	Number of events			
	No decay	$(\tau/m)_{long}$	$(\tau/m)_{medium}$	$(\tau/m)_{short}$
SK-Gd (12.8 - 30.8)	2 (2)	2 [2] (2)	3 [2] (1)	4 [2] (0)
	12 (10)	13 [12] (10)	17 [12] (7)	22 [11] (1)
HK (8.8 - 30.8)	128 (107)	136 [127] (101)	184 [123] (60)	22 [11] (1)
	163 (136)	172 [162] (130)	226 [156] (84)	295 [152] (14)
JUNO (11.3 - 33.3)	20 (17)	21 [20] (16)	28 [19] (10)	37 [19] (2)
	12 (11)	12 [11] (10)	15 [11] (8)	20 [10] (2)

TABLE VI: Number of events associated with inverse-beta decay in SK-Gd, HK and JUNO as well as with $\nu_e - {}^{40}\text{Ar}$ scattering in DUNE. The results, for no decay and with decay, are for the *Fiducial* model. For each experiment, the upper values are for NO, QD; the middle ones for NO, SH (brackets) and the lower ones for IO (brackets). The DSNB detection windows (in MeV) are also shown under each experiment label.

DUNE (Figure 15). Note that we do not show the very low energy range where reactor $\bar{\nu}_e$ and solar ν_e backgrounds dominate over the DSNB signal. Obviously, the comparison of the events shows very similar trends.

Figure 10 shows the predictions for SK-Gd for one-decade running time, both for NO and IO, with backgrounds from invisible muons and charged- and neutral-current interactions induced by atmospheric neutrinos (taken from [78]). Ref. [21] pointed out that neutral-current interactions could hide the DSNB detection window¹².

Figures 11, 14, 15 (upper) and 13 present the expected events for the case of NO. Following the flux behaviors (Figure 6) for NO and QD mass pattern, the number of events in presence are larger than in absence of decay and decrease from $(\tau/m)_{short}$ and $(\tau/m)_{long}$ to the case of no decay, with the results of $(\tau/m)_{medium}$ in between. The events for NO and SH with $(\tau/m)_{short}$ are almost the same as in the case of no decay. When including the

¹² Note that, for the event calculations, we take the detection windows quoted by the Collaborations whenever possible. These can be at variance with the DSNB detection windows visible in our figures.

uncertainty on the core-collapse supernova rate (bands), the most different cases, that is $(\tau/m)_{short}$ and no decay, cannot be distinguished anymore.

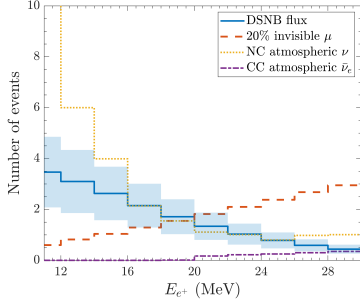


FIG. 10: No decay case: Expected DSNB events, as a function of positron energy, for the *Fiducial* model in the SK-Gd experiment and a running time of 10 years (Table V). The band correspond to the current uncertainty on R_{SN} . Backgrounds from invisible muons, NC and CC atmospheric neutrinos are shown (from [78]). Spallation due to cosmogenic backgrounds (producing for example ${}^9\text{Li}$) and accidentals [12] are not shown.

We take HK as a typical example (upper Figure 12) to show the comparison between the predicted events with no decay and with decay for SH, NO. For the three τ/m values, the differential number of events is practically degenerate with the results in absence of decay. This is in concordance with the findings of [25], but with the quantitative differences mentioned above, that is we find that the use of 2ν instead of the 3ν scenario gives higher (and not lower) number of events by about a few tens of percent.

Figures 11, 14, 15 (lower) present the IO case. Note that the results are below current backgrounds for three experiments. With the background shown, DUNE could have a sensitivity at the lower end of the DSNB detection window. For IO, the event trend is opposite to the one found for NO when going from $(\tau/m)_{long}$ (close to no decay) to $(\tau/m)_{short}$. With $(\tau/m)_{medium}$ the results overlap significantly with no decay, if one includes the current knowledge on R_{SN} . On the contrary, the events could be clearly distinguishable if neutrinos decay with $\tau/m = 10^9$ s/eV.

Table VI presents the total number of events for the four experiments, with/without neutrino decay. For NO when τ/m is short (long) and the mass pattern is SH (QD) the results are practically degenerate with the no decay case. For $(\tau/m)_{short}$ and a QD decay pattern the number of events is always larger than for the no decay case. The largest differences in the number of events appear for IO for which the values for the shortest (τ/m) are a factor of 6 (DUNE) to 10 (JUNO, SK-Gd, HK) smaller than in absence of decay. For $(\tau/m)_{medium}$, whatever is

the mass ordering, the results are in between the ones for $(\tau/m)_{short}$ and $(\tau/m)_{long}$.

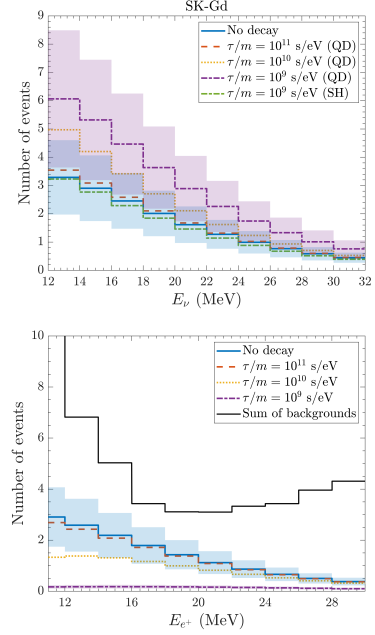


FIG. 11: Expected DSNB $\bar{\nu}_e$ events associated with inverse beta-decay, as a function of positron energy in SK-Gd for a running time of 10 years (see Table V). The cases are NO (upper) and IO (lower figure). The results correspond to the *Fiducial* model with the shortest τ/m (dot-dashed line), the intermediate τ/m (dotted) and the long τ/m (dashed) (decay patterns in Figure 3). For no decay and of $\tau/m = 10^9$ s/eV, the bands come from the uncertainty in the core-collapse supernova rate. The black line corresponds to the summed backgrounds shown in Figure 10.

Before concluding, let us discuss the validity of our results, with respect to the Majorana versus Dirac neutrino nature¹³, which remains unknown (see also the discussion in Ref.[46]). In our calculations we have always assumed that the h.f. contributions are active. First of all, if neutrinos are Majorana particles, it is not meaningful to assign a lepton number to ϕ and Eq.(13) mediates both processes (12) with h.f. $\nu_L \rightarrow \nu_R + \phi$ and the h.c. decays, $\nu_R \rightarrow \nu_R + \phi$ and $\nu_L \rightarrow \nu_L + \phi$. The final states are active neutrinos that are visible in detectors (ν_R are antineutrinos, ν_L neutrinos). If neutrinos are Dirac particles, the new degrees of freedom can be classified with respect to the conserved global (lepton-number) symmetry $U(1)_L$. Our results are also valid for Dirac neutrinos, if one has

¹³ In this discussion, we assume that the heavy neutrinos are relativistic and the limit $m_1/E_{\nu_1} \rightarrow 0$.

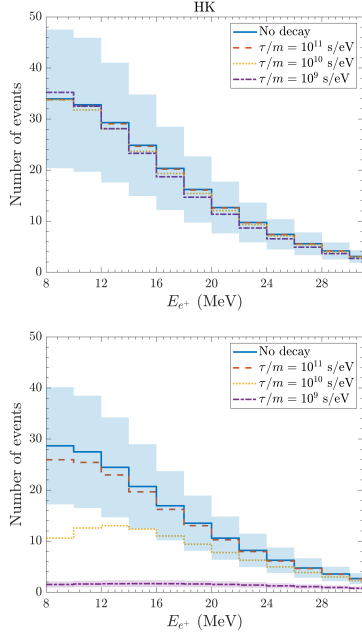


FIG. 12: Expected DSNB $\bar{\nu}_e$ events associated with inverse beta-decay, as a function of positron energy in HK-Gd for a running time of 20 years (see Table V). The cases are NO and SH (upper), IO (lower figure). The results correspond to the *Fiducial* model with the shortest τ/m (dot-dashed line), the intermediate τ/m (dotted) and the long τ/m (dashed). For the cases of no decay case and of $\tau/m = 10^9$ s/eV, the bands come from the uncertainty in the core-collapse supernova rate (see text). Backgrounds are not shown here.

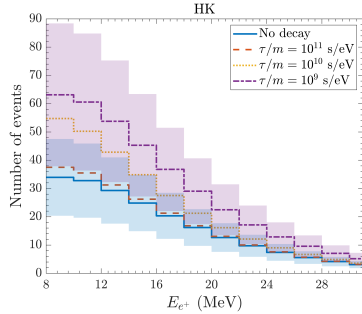


FIG. 13: Same as Figure 12 but for the case of IO.

some combination of lepton-number zero (ϕ_0) and two (ϕ_2) new degrees of freedom. Then, for NO and SH, one could have both an h.c. contribution from $\nu_L \rightarrow \nu_L + \phi_0$ and an h.f. one from $\nu_L \rightarrow \bar{\nu}_R + \phi_2$ where both final states are visible. On the contrary, the h.f. contribution for the former and the h.c. one for the latter produce "wrong helicity" neutrinos that are not visible. For NO and QD the results hold, whatever is the neutrino nature (since there is no $\nu \leftrightarrow \bar{\nu}$ decay). In conclusion, if there

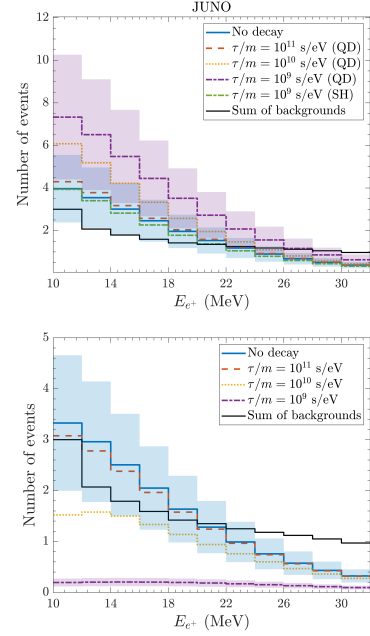


FIG. 14: Same as Figure 10 but for the JUNO detector. The running time is 20 years (Table V).

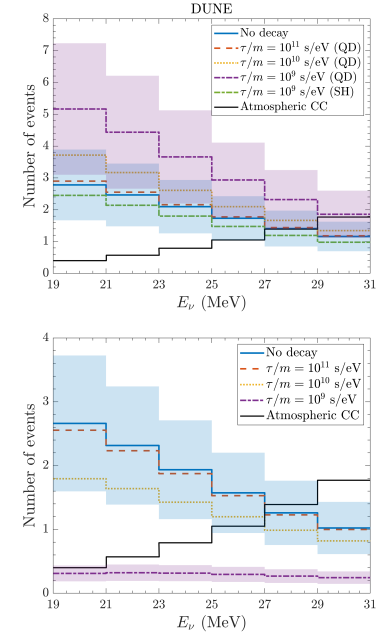


FIG. 15: Number of events associated with ν_e scattering on ^{40}Ar , as a function of neutrino energy, for the DUNE detector. The running time is 20 years (Table V).

is only one new degrees of freedom (either ϕ_0 or ϕ_2), the only case that should be reconsidered is if neutrinos are Dirac particles and if one has NO, SH, or IO, since the

h.f. (for initial decaying neutrinos) and h.c. (for initial decaying antineutrinos) produce "wrong helicity", and therefore sterile, contributions.

IV. CONCLUSIONS

In this work we have investigated the impact of neutrino non-radiative decay on the DSNB. This is the first investigation where a 3ν flavor framework is used with the main astrophysical uncertainties explicitly implemented. These comprise the evolving core-collapse supernova rate and the fraction of dark collapses. We have also implemented the progenitor dependence of the supernova neutrino spectra, using inputs from one-dimensional simulations by the Garching group. We have considered three different scenarios for the black-hole fraction.

The results rely on the solution of the neutrino kinetic equations in presence of ν decay, assuming the decaying eigenstates (considered equal to the mass eigenstates) have *democratic* branching ratios and the same τ/m . We have presented predictions for the DSNB (integrated) fluxes for ν_e and $\bar{\nu}_e$ in presence/absence of ν decay as well as the DSNB differential and total number of events for the running SK-Gd and the upcoming JUNO, DUNE and HK experiments. Note that, for both the fluxes and the events, our results compare well with existing ones with no decay, with 2ν decay and 3ν decay within the same approximations (e.g. one Fermi-Dirac distribution for the neutrino spectra of a single supernova and/or no progenitor dependences or older core-collapse supernova rate).

We have presented a detailed comparison of the results based on the 2ν and 3ν decay framework. If the neutrino mass ordering is normal and the ν mass pattern is strongly hierarchical or quasi-degenerate, the use of both frameworks give similar predictions for the extreme 10^{11} s/eV. On the contrary, if $\tau/m = 10^9$ s/eV ($\tau/m = 10^{10}$) the expected number of events with 2ν decay are underestimated (overestimated) up to about 20 % (30 %), depending on the experiments. The situation is strikingly different if the neutrino mass ordering is inverted, in which case the 3ν framework clearly gives lower predictions by large factors.

More generally, our 3ν results on the DSNB (integrated) fluxes and expected number of events for the four experiments show that, for normal mass ordering and strongly hierarchical mass pattern, if $\tau/m = 10^9$ s/eV,

the events will be essentially degenerate with no decay. This is also the case for the quasi-degenerate mass pattern if $\tau/m = 10^{11}$ s/eV. In contrast, for normal mass ordering and quasi-degenerate mass pattern, if $\tau/m = 10^9$ s/eV, considering neutrinos as stable underestimate the events by almost a factor of 2, whereas $\tau/m = 10^{10}$ s/eV gives results intermediate between the two.

Interestingly, if the neutrino mass ordering is inverted, the results on the events for the intermediate lifetime-to-mass ratio are smaller by a factor of about 2 than in case neutrinos are stable. For the short lifetime-to-mass ratio, the event predictions are clearly distinguishable from no decay, even considering astrophysical uncertainties. It is to be noted that current DSNB predictions can vary by similar factors due to standard physics, with rates up to a factor of 5 smaller than the present SK-I to SK-IV sensitivity [12]. In the unlucky case of non-observation we would not know if this is due to more conservative inputs based on standard physics, or to the fact that neutrinos undergo non-radiative two-body decay with $\tau/m = 10^9$ s/eV.

Obviously, one can envisage several improvements to the present study, such as a more detailed progenitor dependence of the supernova neutrino fluxes, or specific decaying hypothesis from models. Clearly, reducing uncertainties, such as the one from the evolving core-collapse supernova rate appears a key step to extract the most from the DSNB observation.

The upcoming identification of the neutrino mass ordering constitutes a key step in restricting the possible scenarios for the impact of neutrino (in)visible two-body decay on the DSNB. If the mass ordering is normal, the possibility of a low DSNB rate due to neutrino invisible decay with short lifetime-over-mass ratio will be excluded, thus avoiding a potential degeneracy with standard physical inputs.

Clearly, the discovery of the DSNB will bring crucial information for astrophysics and particle physics and will have a unique sensitivity to new physics, such as neutrino decay.

Acknowledgments

The authors wish to thank C. Lunardini, T. Müller, B. Quilain, K. Scholberg and A. Sieverding for providing useful information.

-
- [1] Y. Fukuda *et al.* [Super-Kamiokande], Phys. Rev. Lett. **81** (1998), 1562-1567 [arXiv:hep-ex/9807003 [hep-ex]].
 - [2] Q. R. Ahmad *et al.* [SNO], Phys. Rev. Lett. **87** (2001),

- 071301 [arXiv:nucl-ex/0106015 [nucl-ex]].
- [3] K. Eguchi *et al.* [KamLAND], Phys. Rev. Lett. **90** (2003), 021802 [arXiv:hep-ex/0212021 [hep-ex]].

- [4] K. Hirata *et al.* [Kamiokande-II], Phys. Rev. Lett. **58** (1987), 1490-1493.
- [5] R. M. Bionta, G. Blewitt, C. B. Bratton, D. Casper, A. Ciocio, R. Claus, *et al.* Phys. Rev. Lett. **58** (1987), 1494.
- [6] E. N. Alekseev, L. N. Alekseeva, I. V. Krivosheina and V. I. Volchenko, Phys. Lett. B **205** (1988), 209-214.
- [7] S. Ando and K. Sato, New J. Phys. **6** (2004), 170 [arXiv:astro-ph/0410061 [astro-ph]].
- [8] J. F. Beacom, Ann. Rev. Nucl. Part. Sci. **60** (2010), 439-462 [arXiv:1004.3311 [astro-ph.HE]].
- [9] C. Lunardini, Astropart. Phys. **79** (2016), 49-77 [arXiv:1007.3252 [astro-ph.CO]].
- [10] M. Malek *et al.* [Super-Kamiokande], Phys. Rev. Lett. **90** (2003), 061101 [arXiv:hep-ex/0209028 [hep-ex]].
- [11] H. Zhang *et al.* [Super-Kamiokande], Astropart. Phys. **60** (2015), 41-46 [arXiv:1311.3738 [hep-ex]].
- [12] K. Abe *et al.* [Super-Kamiokande], Phys. Rev. D **104** (2021) no.12, 122002 [arXiv:2109.11174 [astro-ph.HE]].
- [13] A. Gando *et al.* [KamLAND], Astrophys. J. **745** (2012), 193 doi:10.1088/0004-637X/745/2/193 [arXiv:1105.3516 [astro-ph.HE]].
- [14] M. Agostini *et al.* [Borexino], Astropart. Phys. **125** (2021), 102509 [arXiv:1909.02422 [hep-ex]].
- [15] B. Aharmim *et al.* [SNO], Astrophys. J. **653** (2006), 1545-1551 [arXiv:hep-ex/0607010 [hep-ex]].
- [16] C. Lunardini and O. L. G. Peres, JCAP **08** (2008), 033 [arXiv:0805.4225 [astro-ph]].
- [17] A. M. Suliga, J. F. Beacom and I. Tamborra, Phys. Rev. D **105** (2022) no.4, 043008 [arXiv:2112.09168 [astro-ph.HE]].
- [18] S. Ando, K. Sato and T. Totani, Astropart. Phys. **18** (2003), 307-318 [arXiv:astro-ph/0202450 [astro-ph]].
- [19] S. Galais, J. Kneller, C. Volpe and J. Gava, Phys. Rev. D **81** (2010), 053002 [arXiv:0906.5294 [hep-ph]].
- [20] S. Chakraborty, S. Choubey and K. Kar, Phys. Lett. B **702** (2011), 209-215 [arXiv:1006.3756 [hep-ph]].
- [21] A. Priya and C. Lunardini, JCAP **11** (2017), 031 [arXiv:1705.02122 [astro-ph.HE]].
- [22] K. Moller, A. M. Suliga, I. Tamborra and P. B. Denton, JCAP **05** (2018), 066 [arXiv:1804.03157 [astro-ph.HE]].
- [23] S. Horiuchi, K. Sumiyoshi, K. Nakamura, T. Fischer, A. Summa, T. Takiwaki, *et al.*, Mon. Not. Roy. Astron. Soc. **475** (2018) no.1, 1363-1374 [arXiv:1709.06567 [astro-ph.HE]].
- [24] D. Kresse, T. Ertl and H. T. Janka, Astrophys. J. **909** (2021) no.2, 169 [arXiv:2010.04728 [astro-ph.HE]].
- [25] Z. Tabrizi and S. Horiuchi, JCAP **05** (2021), 011 [arXiv:2011.10933 [hep-ph]].
- [26] C. Lunardini, Phys. Rev. Lett. **102** (2009), 231101 [arXiv:0901.0568 [astro-ph.SR]].
- [27] K. Nakazato, E. Mochida, Y. Niino and H. Suzuki, Astrophys. J. **804** (2015) no.1, 75 doi:10.1088/0004-637X/804/1/75 [arXiv:1503.01236 [astro-ph.HE]].
- [28] S. Horiuchi, T. Kinugawa, T. Takiwaki, K. Takahashi and K. Kotake, Phys. Rev. D **103** (2021) no.4, 043003 [arXiv:2012.08524 [astro-ph.HE]].
- [29] J. F. Beacom and M. R. Vagins, Phys. Rev. Lett. **93** (2004), 171101 [arXiv:hep-ph/0309300 [hep-ph]].
- [30] A. Abusleme *et al.* [JUNO], [arXiv:2205.08830 [hep-ex]].
- [31] K. Abe *et al.* [Hyper-Kamiokande], [arXiv:1805.04163 [physics.ins-det]].
- [32] R. Acciarri *et al.* [DUNE], [arXiv:1601.05471 [physics.ins-det]].
- [33] G. J. Mathews, J. Hidaka, T. Kajino and J. Suzuki, Astrophys. J. **790** (2014), 115 [arXiv:1405.0458 [astro-ph.CO]].
- [34] T. S. H. Schilbach, O. L. Caballero and G. C. McLaughlin, Phys. Rev. D **100** (2019) no.4, 043008 [arXiv:1808.03627 [astro-ph.HE]].
- [35] G. J. Mathews, L. Boccioli, J. Hidaka and T. Kajino, Mod. Phys. Lett. A **35** (2020) no.25, 2030011 doi:10.1142/S0217732320300116 [arXiv:1907.10088 [astro-ph.HE]].
- [36] H. Duan, G. M. Fuller and Y. Z. Qian, Ann. Rev. Nucl. Part. Sci. **60** (2010), 569-594 [arXiv:1001.2799 [hep-ph]].
- [37] A. Mirizzi, I. Tamborra, H. T. Janka, N. Saviano, K. Scholberg, R. Bollig, *et al.*, Riv. Nuovo Cim. **39** (2016) no.1-2, 1-112 [arXiv:1508.00785 [astro-ph.HE]].
- [38] S. Horiuchi and J. P. Kneller, J. Phys. G **45** (2018) no.4, 043002 [arXiv:1709.01515 [astro-ph.HE]].
- [39] C. Volpe, Int. J. Mod. Phys. E **24** (2015) no.09, 1541009 [arXiv:1506.06222 [astro-ph.SR]].
- [40] L. Wolfenstein, Phys. Rev. D **17** (1978), 2369-2374.
- [41] S. P. Mikheev and A. Y. Smirnov, Nuovo Cim. C **9** (1986), 17-26.
- [42] K. Nakazato, Phys. Rev. D **88** (2013) no.8, 083012 [arXiv:1306.4526 [astro-ph.HE]].
- [43] M. C. Gonzalez-Garcia and M. Maltoni, Phys. Lett. B **663** (2008), 405-409 [arXiv:0802.3699 [hep-ph]].
- [44] J. M. Berryman, A. de Gouvea and D. Hernandez, Phys. Rev. D **92** (2015) no.7, 073003 [arXiv:1411.0308 [hep-ph]].
- [45] B. Aharmim *et al.* [SNO], Phys. Rev. D **99** (2019) no.3, 032013 [arXiv:1812.01088 [hep-ex]].
- [46] A. de Gouvêa, I. Martinez-Soler and M. Sen, Phys. Rev. D **101** (2020) no.4, 043013 [arXiv:1910.01127 [hep-ph]].
- [47] M. Kachelriess, R. Tomas and J. W. F. Valle, Phys. Rev. D **62** (2000), 023004 [arXiv:hep-ph/0001039 [hep-ph]].
- [48] Y. Farzan, Phys. Rev. D **67** (2003), 073015 [arXiv:hep-ph/0211375 [hep-ph]].
- [49] M. Escudero and M. Fairbairn, Phys. Rev. D **100** (2019) no.10, 103531 [arXiv:1907.05425 [hep-ph]].
- [50] J. M. Berryman, A. de Gouvêa, D. Hernández and R. L. N. Oliveira, Phys. Lett. B **742** (2015), 74-79 [arXiv:1407.6631 [hep-ph]].
- [51] D. S. Chattopadhyay, K. Chakraborty, A. Dighe, S. Goswami and S. M. Lakshmi, Phys. Rev. Lett. **129** (2022) no.1, 011802 [arXiv:2111.13128 [hep-ph]].
- [52] S. Ando, Phys. Lett. B **570** (2003), 11 [arXiv:hep-ph/0307169 [hep-ph]].
- [53] G. L. Fogli, E. Lisi, A. Mirizzi and D. Montanino, Phys. Rev. D **70** (2004), 013001 [arXiv:hep-ph/0401227 [hep-ph]].
- [54] A. De Gouvêa, I. Martinez-Soler, Y. F. Perez-Gonzalez and M. Sen, Phys. Rev. D **102** (2020), 123012 [arXiv:2007.13748 [hep-ph]].
- [55] M. T. Keil, G. G. Raffelt and H. T. Janka, Astrophys. J.

- 590** (2003), 971-991 [arXiv:astro-ph/0208035 [astro-ph]].
- [56] A. S. Dighe and A. Y. Smirnov, Phys. Rev. D **62** (2000), 033007 [arXiv:hep-ph/9907423 [hep-ph]].
 - [57] H. Duan and J. P. Kneller, J. Phys. G **36** (2009), 113201 [arXiv:0904.0974 [astro-ph.HE]].
 - [58] J. Barranco, A. Bernal and D. Delepine, J. Phys. G **45** (2018) no.5, 055201 [arXiv:1706.03834 [astro-ph.CO]].
 - [59] E. Di Valentino, O. Mena, S. Pan, L. Visinelli, W. Yang, A. Melchiorri, *et al.*, Class. Quant. Grav. **38** (2021) no.15, 153001 [arXiv:2103.01183 [astro-ph.CO]].
 - [60] E. E. Salpeter, Astrophys. J. **121** (1955), 161-167.
 - [61] J. J. Ziegler, T. D. P. Edwards, A. M. Suliga, I. Tamborra, S. Horiuchi, S. Ando and K. Freese, [arXiv:2205.07845 [astro-ph.GA]].
 - [62] H. Yuksel, M. D. Kistler, J. F. Beacom and A. M. Hopkins, Astrophys. J. Lett. **683** (2008), L5-L8 [arXiv:0804.4008 [astro-ph]].
 - [63] P. Madau and M. Dickinson, Ann. Rev. Astron. Astrophys. **52** (2014), 415-486 [arXiv:1403.0007 [astro-ph.CO]].
 - [64] I. K. Baldry and K. Glazebrook, Astrophys. J. **593** (2003), 258-271 [arXiv:astro-ph/0304423 [astro-ph]].
 - [65] S. Horiuchi, J. F. Beacom and E. Dwek, Phys. Rev. D **79** (2009), 083013 doi:10.1103/PhysRevD.79.083013 [arXiv:0812.3157 [astro-ph]].
 - [66] S. Horiuchi, J. F. Beacom, C. S. Kochanek, J. L. Prieto, K. Z. Stanek and T. A. Thompson, Astrophys. J. **738** (2011), 154-169 doi:10.1088/0004-637X/738/2/154 [arXiv:1102.1977 [astro-ph.CO]].
 - [67] C. Lunardini, Astropart. Phys. **26** (2006), 190-201 [arXiv:astro-ph/0509233 [astro-ph]].
 - [68] K. Sumiyoshi, S. Yamada and H. Suzuki, Astrophys. J. **667** (2007), 382-394 [arXiv:0706.3762 [astro-ph]].
 - [69] L. Hudepohl, Munich, Tech. U. (2013).
 - [70] C. W. Kim and W. P. Lam, Mod. Phys. Lett. A **5** (1990), 297-299.
 - [71] P. A. Zyla *et al.* [Particle Data Group], PTEP **2020** (2020) no.8, 083C01
 - [72] J. F. Beacom and N. F. Bell, Phys. Rev. D **65** (2002), 113009 [arXiv:hep-ph/0204111 [hep-ph]].
 - [73] F. Capozzi, E. Di Valentino, E. Lisi, A. Marrone, A. Melchiorri and A. Palazzo, Phys. Rev. D **104** (2021) no.8, 083031 [arXiv:2107.00532 [hep-ph]].
 - [74] B. Quilain, Private communication.
 - [75] F. An *et al.* [JUNO], J. Phys. G **43** (2016) no.3, 030401 [arXiv:1507.05613 [physics.ins-det]].
 - [76] A. Strumia and F. Vissani, Phys. Lett. B **564** (2003), 42-54 [arXiv:astro-ph/0302055 [astro-ph]].
 - [77] G. Martinez-Pinedo and A. Sieverding, Private communication.
 - [78] H. Kunxian, PhD Thesis, Kyoto University (2015).